Texts

S1. HONO observational datasets and model evaluation methods

To evaluate the model performance across different land covers and emission conditions, we collected a comprehensive dataset of 96 global HONO observation campaigns. These include 32 urban, 23 suburban, 16 rural, 22 coastal, and 3 marine field observations. Table S1 details the geographical locations, observation periods, instruments, and data sources for each field campaign, along with the mean concentrations of HONO, NO_2, and HONO/NO_2 ratios. Overall, measured HONO levels are strongly influenced by anthropogenic emissions, with average concentrations decreasing in the order of urban, suburban, rural, coastal, and marine environments.

For spatial matching, each observation site was assigned to the nearest model grid cell based on its coordinates. We extracted the simulated results from the lowest model layer (approximately 992.56 hPa). Due to the scarcity of long-term global HONO measurements, we compared observations collected between 1998 and 2024 against the simulated monthly means for the corresponding months in our target year (2019). For observations spanning multiple months, the data were allocated to the month containing the majority of the sampling days. To evaluate HONO diurnal variations, we extracted mean hourly HONO data from the previous observation studies. These diurnal data were averaged according to four site types and four groups of months: December–January–February (DJF), March–April–May (MAM), June–July–August (JJA), and September–October–November (SON) (Figure S1). The results were then compared with the 1-hour resolution output from CESM2-SLH-HONO. Since the model uses Coordinated Universal Time (UTC), the simulated time was converted to local solar time based on the longitude of each site prior to the diurnal pattern comparison.

Figures

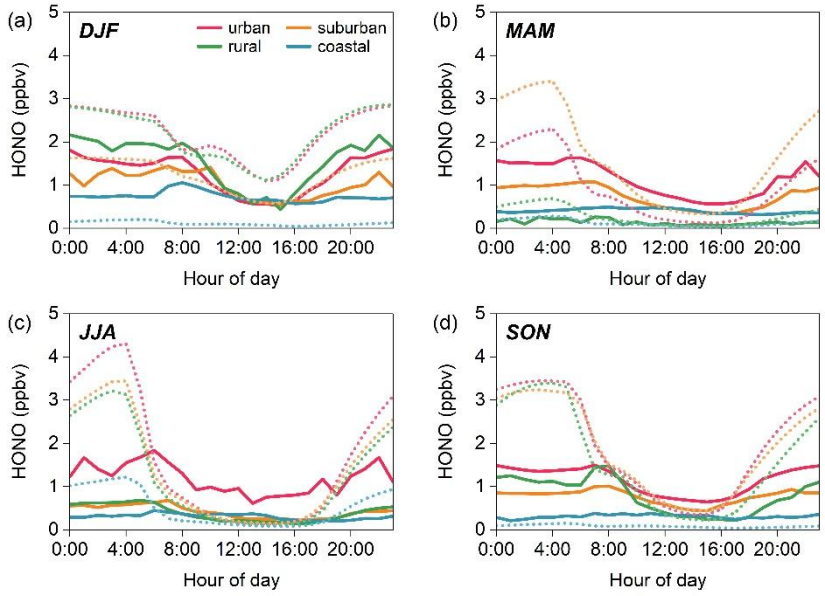


Figure S1: Comparison of mean diurnal HONO variations at urban, suburban, rural, and coastal sites between observations and the Standard simulation. Panels (a)–(d) represent DJF (December–January–February), MAM (March–April–May), JJA (June–July–August), and SON (September–October–November), respectively. Solid and dotted lines represent observations and simulations, respectively.

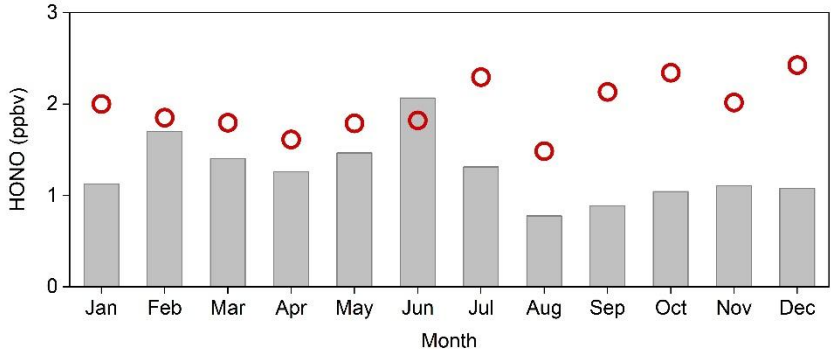


Figure S2: Comparison of observed and simulated monthly HONO concentrations in Beijing for 2019. The gray bars represent the observed monthly HONO concentrations at the Beijing site, based on the measurements reported by Zhang et al. (2025), while the red circles denote the corresponding simulated monthly HONO concentrations.

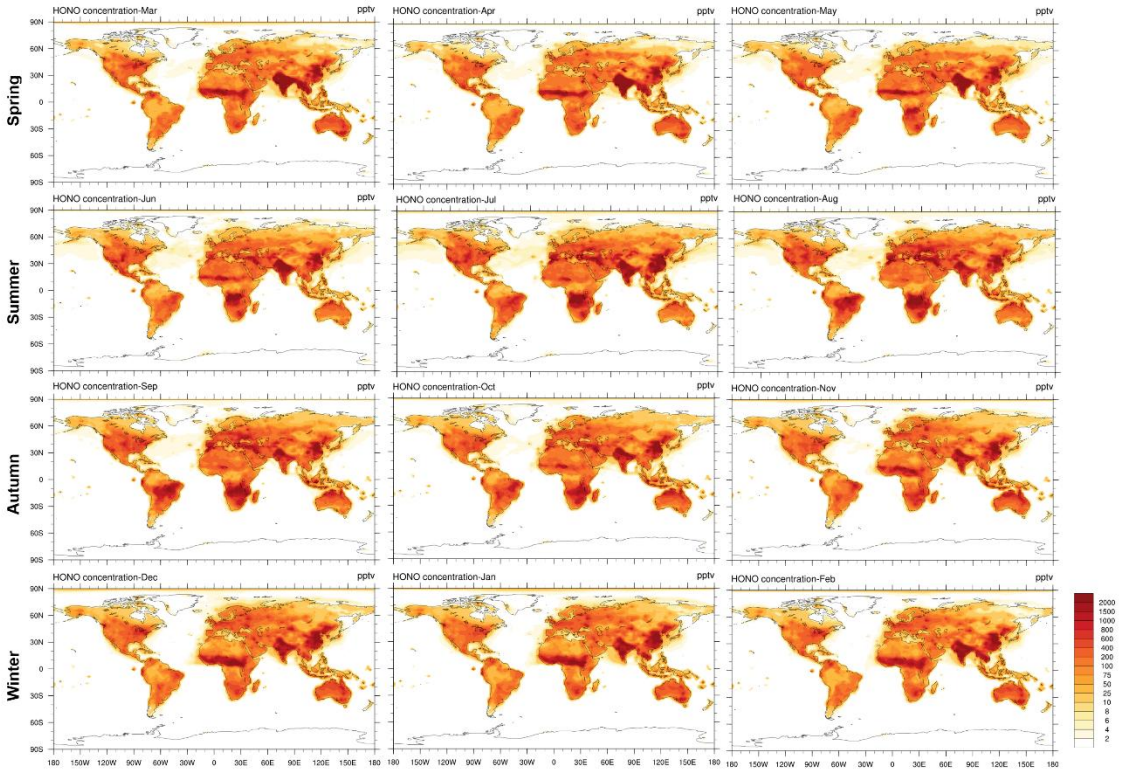


Figure S3: Global horizontal distributions of monthly average HONO mixing ratio at the surface in 2019.

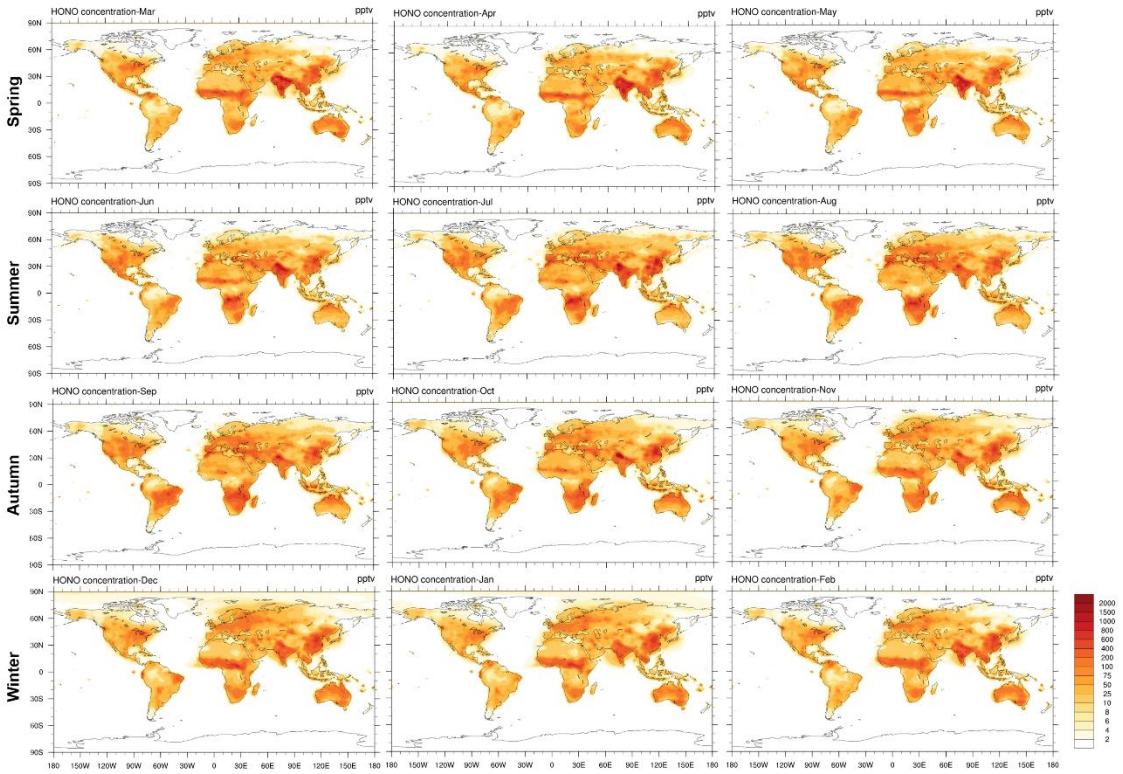


Figure S4: Global horizontal distributions of monthly average HONO mixing ratio within the boundary layer in 2019.

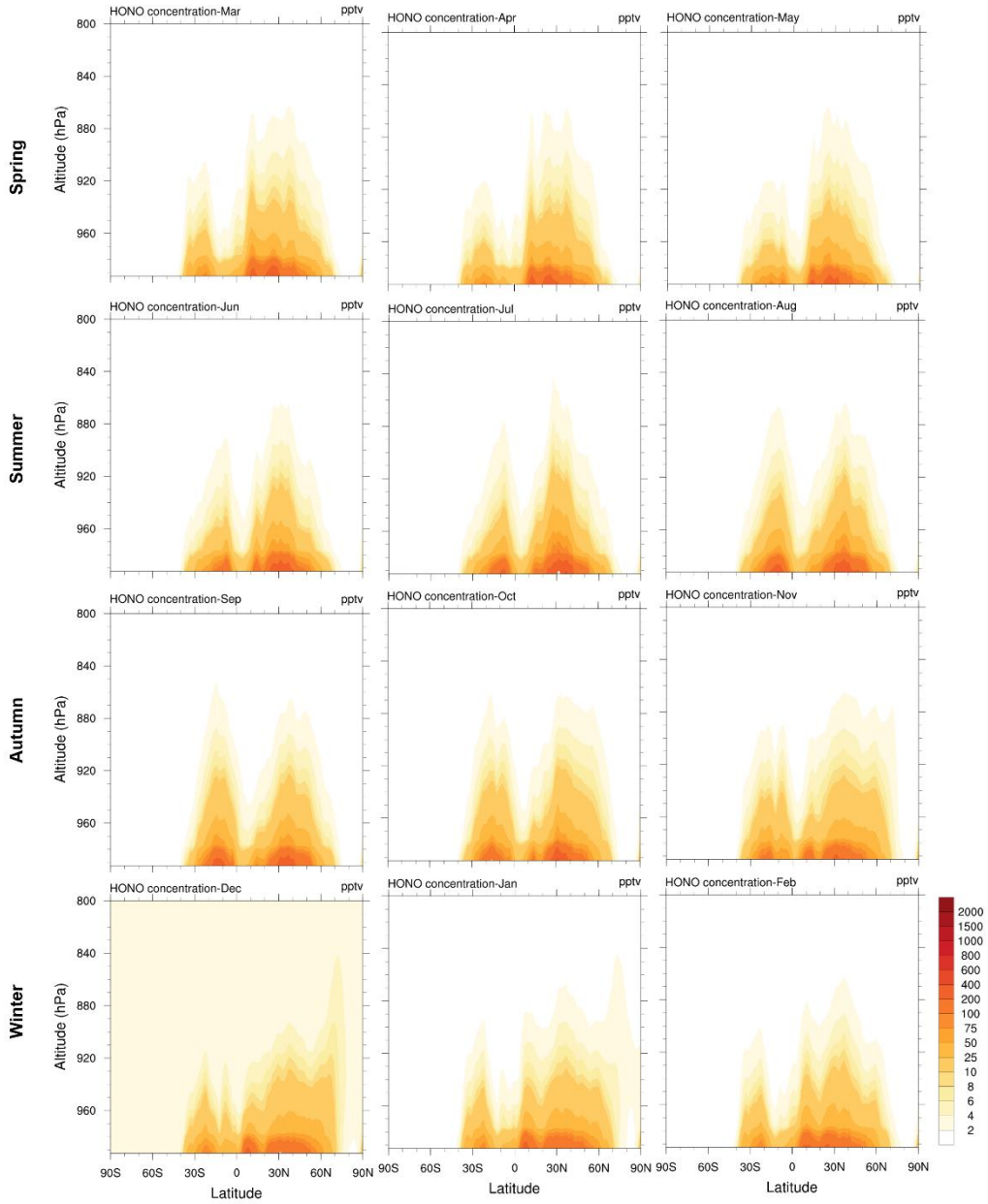


Figure S5: Global vertical distributions of monthly average HONO mixing ratio with latitudinal mean in 2019.

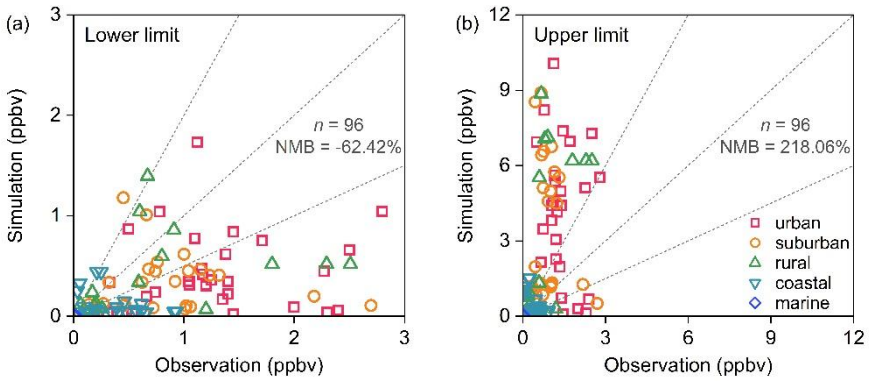


Figure S6: Comparison of the observed and simulated surface HONO concentrations for (a) Lower-limit and (b) Upper-limit sensitivity simulations. Each point represents an observation simulation pair for an individual site, including urban, suburban, rural, coastal, and marine sites. The gray dashed lines indicate simulation to observation ratios of 1:2, 1:1, and 2:1.

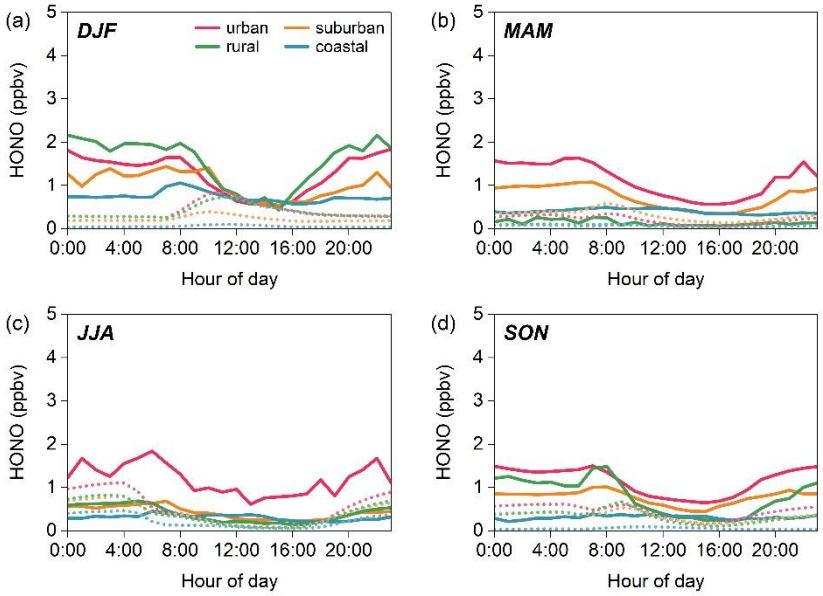


Figure S7: Comparison of mean diurnal HONO variations at urban, suburban, rural, and coastal sites between observations and the Lower-limit simulation, grouped by (a) DJF, (b) MAM, (c) JJA, and (d) SON. Solid and dotted lines represent observations and simulations, respectively.

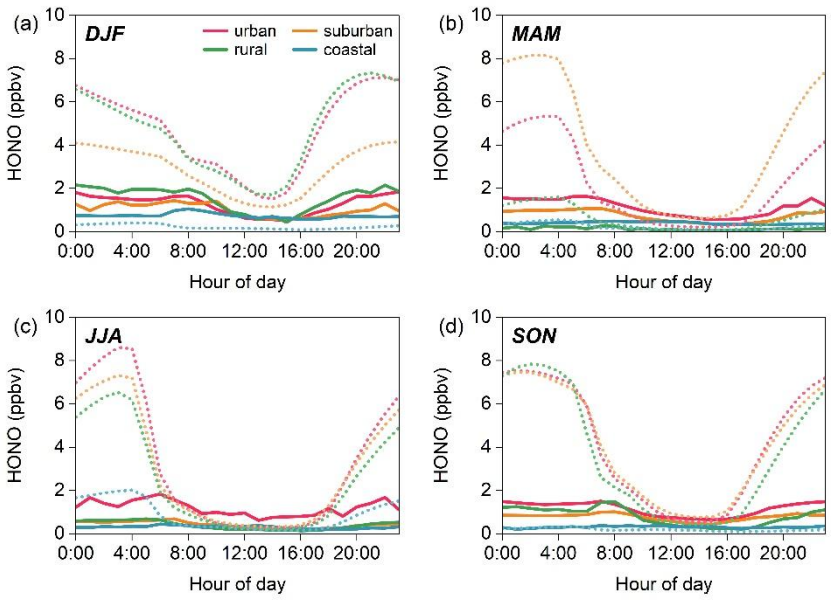


Figure S8: Comparison of mean diurnal HONO variations at urban, suburban, rural, and coastal sites between observations and the Upper-limit simulation, grouped by (a) DJF, (b) MAM, (c) JJA, and (d) SON. Solid and dotted lines represent observations and simulations, respectively.

Tables

Table S1: Summary of observational datasets of HONO and NO_2 concentrations and HONO/NO_2 ratios across diverse environments worldwide used for model evaluation. The complete table is provided as a separate Excel file (Table_S1.xlsx).

Table S2: Comparison of observed and simulated surface HONO concentrations (mean ± standard deviation) and normalized mean bias (NMB) for different site types under the Standard, Lower-limit, and Upper-limit simulations.

Site type	*N*	Observed HONO (ppbv)	Simulated HONO (ppbv)			NMB (%)		
			Standard	Lower-limit	Upper-limit	Standard	Lower-limit	Upper-limit
Urban	32	1.26 ± 0.67	1.73 ± 1.38	0.42 ± 0.38	3.62 ± 2.80	37.51	-66.45	187.71
Suburban	23	0.91 ± 0.58	1.58 ± 1.22	0.35 ± 0.29	3.54 ± 2.75	74.22	-61.00	289.98
Rural	16	0.78 ± 0.79	1.62 ± 1.54	0.41 ± 0.40	3.35 ± 3.17	108.97	-46.94	331.14
Coastal	22	0.38 ± 0.27	0.25 ± 0.30	0.12 ± 0.13	0.44 ± 0.47	-32.98	-69.64	16.27
Marine	3	0.0035 ± 0.0046	0.0045 ± 0.0012	0.0040 ± 0.0013	0.0092 ± 0.0011	28.70	13.30	163.17

Table S3: Pearson correlation coefficients (*r*) between observed and simulated HONO diurnal variations under the Standard case for different site types in DJF, MAM, JJA, and SON.

Site type	DJF	MAM	JJA	SON
Urban	0.90	0.85	0.67	0.91
Suburban	0.72	0.85	0.68	0.73
Rural	0.88	0.64	0.90	0.77
Coastal	0.24	0.06	0.03	-0.01

Table S4: Monthly variation and annual average of the global tropospheric burden of HONO in 2019.

Month	HONO burden (Gg N)
Jan	18.7
Feb	18.2
Mar	19.3
Apr	19.0
May	18.4
Jun	20.1
Jul	24.7
Aug	23.1
Sep	22.3
Oct	21.4
Nov	19.4
Dec	19.8
Annual average	20.4

Table S5: Annual HONO production from different sources under the Lower-limit and Upper-limit simulations in 2019.

HONO sources	Lower-limit (Tg N/yr)	Upper-limit (Tg N/yr)
Emission	6.0	19.2
Homogeneous source	19.8	22.0
Heterogeneous source	2.2	17.7
Particulate nitrate photolysis	3.1	10.5

References

Zhang, Y., Liu, Y., Ma, W., Hua, C., Zheng, F., Lian, C., Wang, W., Xia, M., Zhao, Z., Li, J., Xie, J., Wang, Z., Wang, Y., Chen, X., Zhang, Y., Feng, Z., Yan, C., Chu, B., Du, W., Kerminen, V.-M., Bianchi, F., Petäjä, T., Worsnop, D., and Kulmala, M.: Changing aerosol chemistry is redefining HONO sources, Nat. Commun., 16, 5238, https://doi.org/10.1038/s41467-025-60614-7, 2025.